Acta Mech Sin (2009) 25:491–497
DOI 10.1007/s10409-009-0260-8

RESEARCH PAPER

On the contact width in generalized plain strain JKR model for isotropic solids

Cong Yan · Shaohua Chen

Received: 1 September 2008 / Revised: 23 March 2009 / Accepted: 9 April 2009 / Published online: 15 May 2009

Abstract Adhesive contact model between an elastic cylinder and an elastic half space is studied in the present paper, in which an external pulling force is acted on the above cylinder with an arbitrary direction and the contact width is assumed to be asymmetric with respect to the structure. Solutions to the asymmetric model are obtained and the effect of the asymmetric contact width on the whole pulling process is mainly discussed. It is found that the smaller the absolute value of Dundurs' parameter β or the larger the pulling angle θ, the more reasonable the symmetric model would be to approximate the asymmetric one.

Keywords Contact mechanics · Generalized JKR model · Asymmetric contact width · Oscillatory solution · Non-oscillatory solution

1 Introduction

Contact mechanics has been widely applied in many branches of engineering since Hertz [1] gave the famous Hertz solution in 1882. In the later experiments [2,3], it was found that at low loads contact areas were considerably larger than those predicted by Hertz and tended towards a constant finite value as the load was reduced to zero. Molecular interactions between contacting objects should be incorporated into contact mechanics models. Johnson et al. [2] developed the classical JKR model of adhesive contact based on a balance between elastic and surface energies and predicted a compressive stress field near the central region of contact and a singular tensile stress field near the contact edges. On the other hand, Derjaguin et al. [4] proposed the classical DMT model in which the stress field remains in the Hertz profile within the contact region while intermolecular adhesion is assessed outside the contact area. Maugis [5] developed a more general model and successfully connected the JKR and DMT models through a cohesive model of adhesive contact.

In recent years, contact mechanics is also becoming a valuable platform to study biological adhesion systems such as cell–cell contact [6,7], cells on stretched substrates [8], as well as adhesion systems of gecko and insects [9–16]. In most of the adhesive contact models, the external force is normal to the contact interface, which allows us to conclude immediately that the contact area is symmetric with respect to the contact model. However, in order to simulate some special state of bio-adhesive tissues or bio-experiments, such as geckoes climbing on a wall or titled micro-pipette technology to measure the adhesive force between cells, the external force is titled to the contact interface, what effect will happen to the contact area? Is the contact width in the plain strain model still symmetric with respect to the axis of the contact model?

A plain strain generalized JKR model of an elastic cylinder subjected to an external force in an arbitrary direction, in adhesive contact with an elastic half space, has been investigated by Chen and Wang [17], in which the contact region is assumed to be symmetric with respect to the studied structure. Actually, this assumption is not strictly correct because it will result in asymmetric energy release rates at two contact edges due to the oscillatory characteristics of the contact pressure.

In the present paper, the assumption of symmetric contact width is given up and the adhesive contact model in Ref. [17]

The project supported by the National Natural Science Foundation of China (10672165, 10732050, 10721202), KJCX2-YW-M04, CAS Innovation Program and Start Fund for Returning Overseas person.

C. Yan · S. Chen (✉)
LNM, Institute of Mechanics, Chinese Academy of Sciences, 100190 Beijing, China
e-mail: chenshaohua72@hotmail.com

is investigated further. Exact solutions to the present contact model are obtained and the influences of the symmetric assumption on the final solutions are mainly discussed.

2 Adhesive contact model

The asymmetric model of an elastic cylinder of radius R in adhesive contact with an elastic half space is studied in the present paper as shown in Fig. 1, in which an external force F in an arbitrary direction, θ, is acted to pull the above cylinder. (E_1, ν_1) and (E_2, ν_2) denote the Young's moduli and Poisson ratios of the upper cylinder and lower half space, respectively. The contact region is assumed to be perfect bonding with a contact length a on the right side and b on the left one. (x, y_1) and (x, y_2) are two Cartesian coordinate systems with y_1 and y_2 pointing into the upper and the lower solids, respectively. Due to the assumption of perfect bonding, the edges of the contact region resemble two opposing interfacial cracks under plane strain deformation.

As in almost all contact mechanics theories [19], the contact width $a + b$ is assumed to be much smaller compared to the radius of the cylinder R. The pulling force is assumed to be properly added such that no net bending moment on the contact region is produced. This assumption is not trivial and accepted by almost all literatures in the field of contact mechanics, which can be actually realized in experiments, such as Ref. [19].

3 Solutions to the contact model

On the basis of the above model, we can express the continuity condition of displacements across the contact interface as

$$\begin{aligned} &\bar{u}_{x1} - \bar{u}_{x2} = 0, \\ &\bar{u}_{y1} + \bar{u}_{y2} = \delta - \frac{x^2}{2R}, \end{aligned} \qquad -b < x < a, \tag{1}$$

where $\bar{u}_{x1}$ and $\bar{u}_{x2}$ ($\bar{u}_{y1}$ and $\bar{u}_{y2}$) denote the displacements of the contact surface in the x ($y_i, i = 1, 2$) direction of the above and lower materials, respectively; δ is the relative central displacement, which has the same definition as Ref. [18]. Assumption of parabolic shape of the upper cylinder yields the second term on the right side in the second equation.

Differentiating Eq. (1) with respect to x yields

$$\begin{aligned} &\frac{\partial \bar{u}_{x1}}{\partial x} - \frac{\partial \bar{u}_{x2}}{\partial x} = 0, \\ &\frac{\partial \bar{u}_{y1}}{\partial x} + \frac{\partial \bar{u}_{y2}}{\partial x} = -\frac{x}{R}, \end{aligned} \qquad -b < x < a. \tag{2}$$

The surface displacement of an elastic half-space can be related to the surface tractions via Green functions of an elastic half space. When this is done, Eq. (2) leads to two coupled integral equations,

$$\begin{aligned} &\frac{1}{\pi}\int_{-b}^{a} \frac{Q(s)}{s-x}\mathrm{d}s - \beta P(x) = 0, \\ &\frac{1}{\pi}\int_{-b}^{a} \frac{P(s)}{s-x}\mathrm{d}s + \beta Q(x) = -\frac{E^* x}{2R}, \end{aligned} \tag{3}$$

where $P(x)$ and $Q(x)$ denote the normal and tangential tractions along the contact interface of the cylinder, respectively. The generalized effective modulus E^* is

$$\frac{1}{E^*} = \frac{1-v_1^2}{E_1} + \frac{1-v_2^2}{E_2} \tag{4}$$

and

$$\beta = \frac{1}{2}\left\{\frac{(1-2v_1)/\mu_1 - (1-2v_2)/\mu_2}{(1-v_1)/\mu_1 + (1-v_2)/\mu_2}\right\} \tag{5}$$

is one of the Dundurs' parameter [20]. μ_1 and μ_2 are the shear moduli of materials. Rewriting Eq. (3) in a matrix form

$$\frac{1}{\pi}\int_{-b}^{a} \frac{\boldsymbol{A}}{s-x}\boldsymbol{f}(s)\mathrm{d}s + \boldsymbol{B}\boldsymbol{f}(x) = \boldsymbol{C}\,, \tag{6}$$

where the coefficients of matrices are

$$\begin{aligned} &\boldsymbol{f}(s) = \begin{bmatrix} Q(s) \\ P(s) \end{bmatrix}, \quad \boldsymbol{A} = \begin{bmatrix} 1 & 0 \\ 0 & 1 \end{bmatrix} = \boldsymbol{I}\,, \\ &\boldsymbol{B} = \begin{bmatrix} 0 & -\beta \\ \beta & 0 \end{bmatrix}, \quad \boldsymbol{C} = \begin{bmatrix} 0 \\ \dfrac{-E^* x}{2R} \end{bmatrix}. \end{aligned} \tag{7}$$

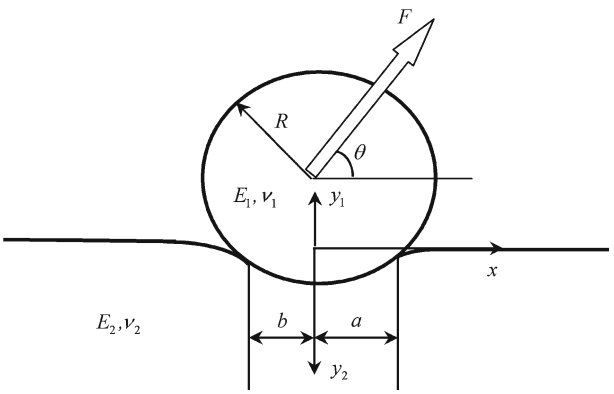

Fig. 1 Plane strain model of an elastic cylinder adhesively contacting with an elastic half plane. F is an external pulling force and θ the pulling angle. (E_1, ν_1) and (E_2, ν_2) are the Young's moduli and Poisson ratios of the cylinder and the half plane, respectively. R is the radius of the cylinder. b is the left contact width and a is the right one

Introducing the following transformation

$$F_k(z) = \frac{1}{2\pi \mathrm{i}} \int_{-b}^{a} \frac{f_k(s)}{s - z} \mathrm{d}s, \qquad k = 1, 2, \tag{8}$$

where $z = x + y\mathrm{i}$ and $\mathrm{i} = \sqrt{-1}$. Equation (6) can be transferred to two inhomogeneous Hilbert equations. Solving the Hilbert equations and combining the boundary conditions

$$\int_{-b}^{a} P(x)\mathrm{d}x = -F\sin\theta, \quad \int_{-b}^{a} Q(x)\mathrm{d}x = -F\cos\theta \tag{9}$$

yields the interfacial tractions. The calculations are quite lengthy but the methodology to solve the two inhomogeneous Hilbert equations is standard, which can be referenced in Ref. [8]. We skip the details and present the final interfacial tractions $P(x)$ and $Q(x)$ in the contact region directly,

$$P(x) = -2\mathrm{Im}\{I(x)\} - \mathrm{Re}\left\{\frac{(F\sin\theta + \mathrm{i}F\cos\theta)(b+x)^{-\bar{r}}(a-x)^{-r}}{\pi\sqrt{1-\beta^2}}\right\}, \tag{10}$$

$$Q(x) = 2\mathrm{Re}\{I(x)\} + \frac{E^*\beta x}{2R(1-\beta^2)} - \mathrm{Im}\left\{\frac{(F\sin\theta + \mathrm{i}F\cos\theta)(b+x)^{-\bar{r}}(a-x)^{-r}}{\pi\sqrt{1-\beta^2}}\right\}, \tag{11}$$

where

$$I(x) = \frac{E^*(b+x)^{-\bar{r}}(a-x)^{-r}}{4\pi R\mathrm{i}(1-\beta^2)} \int_{-b}^{a} \frac{t(b+t)^{\bar{r}}(a-t)^{r}}{t-x}\mathrm{d}t. \tag{12}$$

From the interfacial tractions (10) and (11), we find that the stress singularity r is oscillatory with an oscillatory index ε,

$$r = \frac{1}{2} + \mathrm{i}\varepsilon, \qquad \varepsilon = \frac{1}{2\pi}\ln\frac{1+\beta}{1-\beta}. \tag{13}$$

Introducing a complex-valued stress intensity factor, for the right contact edge at $x = a$, we have

$$K^{\mathrm{R}} = -\sqrt{2\pi}\lim_{x\to a}(a-x)^{r}[P(x) + \mathrm{i}Q(x)]. \tag{14}$$

Substituting Eqs. (10) and (11) into the above equation yields the stress intensity factor at the right contact edge

$$K^{\mathrm{R}} = \frac{E^*(a+b)^{-\bar{r}}}{\sqrt{2\pi}R(1-\beta^2)} \int_{-b}^{a} \frac{t(b+t)^{\bar{r}}(a-t)^{r}}{a-t}\mathrm{d}t + \frac{\sqrt{2}(a+b)^{-\bar{r}}(F\sin\theta + \mathrm{i}F\cos\theta)}{\sqrt{\pi(1-\beta^2)}}. \tag{15}$$

Similarly, substituting Eqs. (10) and (11) into the following expression

$$K^{\mathrm{L}} = -\sqrt{2\pi}\lim_{x\to -b}(b+x)^{\bar{r}}[P(x) + \mathrm{i}Q(x)] \tag{16}$$

leads to the stress intensity factor at the left contact edge $x = -b$

$$K^{\mathrm{L}} = \frac{E^*(a+b)^{-r}}{\sqrt{2\pi}R(1-\beta^2)} \int_{-b}^{a} \frac{t(b+t)^{\bar{r}}(a-t)^{r}}{-(b+t)}\mathrm{d}t + \frac{\sqrt{2}(a+b)^{-r}(F\sin\theta + \mathrm{i}F\cos\theta)}{\sqrt{\pi(1-\beta^2)}}. \tag{17}$$

At equilibrium, the dynamic Griffith energy balance criterion is used for the right and left contact edges, respectively, i.e.

$$\begin{aligned} G^{\mathrm{R}} &= \frac{1}{\cosh^2\pi\varepsilon}\frac{|K^{\mathrm{R}}|^2}{2E^*} = \Delta\gamma, \\ G^{\mathrm{L}} &= \frac{1}{\cosh^2\pi\varepsilon}\frac{|K^{\mathrm{L}}|^2}{2E^*} = \Delta\gamma, \end{aligned} \tag{18}$$

which yield two governing equations describing the relation among the external pulling force F, pulling angle θ and the contact width $a + b$,

$$\begin{aligned} &\frac{2(F^{\mathrm{R}})^2}{\pi(1-\beta^2)(a+b)} - \frac{2F^{\mathrm{R}}E^*\mathrm{sech}(\pi\varepsilon)}{(1-\beta^2)^{3/2}R} \\ &\times\left\{\sin\theta\left[\frac{(a+b)}{8}(1+4\varepsilon^2) - \frac{a}{2}\right] + a\varepsilon\cos\theta\right\} \\ &+ \frac{\pi E^{*^2}\mathrm{sech}^2(\pi\varepsilon)(a+b)}{2R^2(1-\beta^2)^2} \\ &\times\left\{\left[\frac{(a+b)}{8}(1+4\varepsilon^2) - \frac{a}{2}\right]^2 + a^2\varepsilon^2\right\} \\ &- 2E^*\Delta\gamma\cosh^2(\pi\varepsilon) = 0, \end{aligned} \tag{19}$$

and

$$\begin{aligned} &\frac{2(F^{\mathrm{L}})^2}{\pi(1-\beta^2)(a+b)} - \frac{2F^{\mathrm{L}}E^*\mathrm{sech}(\pi\varepsilon)}{(1-\beta^2)^{3/2}R} \\ &\times\left\{\sin\theta\left[\frac{(a+b)}{8}(1+4\varepsilon^2) - \frac{b}{2}\right] - b\varepsilon\cos\theta\right\} \\ &+ \frac{\pi E^{*^2}\mathrm{sech}^2(\pi\varepsilon)(a+b)}{2R^2(1-\beta^2)^2} \\ &\times\left\{\left[\frac{(a+b)}{8}(1+4\varepsilon^2) - \frac{b}{2}\right]^2 + b^2\varepsilon^2\right\} \\ &- 2E^*\Delta\gamma\cosh^2(\pi\varepsilon) = 0, \end{aligned} \tag{20}$$

where F^{R} corresponds to the energy balance at the right contact edge and F^{L} corresponds to that at the left one.

Normalized pulling force as functions of the contact width $a + b$ and pulling angle θ can be obtained explicitly from

Eqs. (19) and (20) as

$$\frac{F^{\mathrm{R}}}{\Delta\gamma} = \frac{\pi}{2(1-\beta^2)^{1/2}}\frac{E^*R}{\Delta\gamma}\frac{(a+b)}{R} \times\left\{\sin\theta\left[\frac{(1+4\varepsilon^2)}{8}\frac{(a+b)}{R} - \frac{a+b}{2R}\frac{1}{1+\frac{1}{\lambda}}\right] + \frac{a+b}{R}\frac{\varepsilon\cos\theta}{1+\frac{1}{\lambda}}\right\} + \sqrt{A_1}, \tag{21}$$

and

$$\frac{F^{\mathrm{L}}}{\Delta\gamma} = \frac{\pi}{2(1-\beta^2)^{1/2}}\frac{E^*R}{\Delta\gamma}\frac{(a+b)}{R} \times\left\{\sin\theta\left[\frac{(1+4\varepsilon^2)}{8}\frac{(a+b)}{R} - \frac{a+b}{2R}\frac{1}{1+\lambda}\right] - \frac{a+b}{R}\frac{\varepsilon\cos\theta}{1+\lambda}\right\} + \sqrt{A_2}, \tag{22}$$

where

$$A_1 = \pi\cosh^4(\pi\varepsilon)(1-\beta^2)\frac{E^*R}{\Delta\gamma}\frac{(a+b)}{R} + \frac{\pi^2}{4(1-\beta^2)}\left(\frac{E^*R}{\Delta\gamma}\right)^2\left(\frac{a+b}{R}\right)^2 \times\left\{\left\{\sin\theta\left[\frac{(1+4\varepsilon^2)}{8}\frac{(a+b)}{R} - \frac{a+b}{2R}\frac{1}{1+\frac{1}{\lambda}}\right] + \frac{a+b}{R}\frac{\varepsilon\cos\theta}{1+\frac{1}{\lambda}}\right\}^2 - \left[\frac{(1+4\varepsilon^2)}{8}\frac{(a+b)}{R} - \frac{a+b}{2R}\frac{1}{1+\frac{1}{\lambda}}\right]^2 - \left(\frac{a+b}{R}\frac{\varepsilon}{1+\frac{1}{\lambda}}\right)^2\right\}, \tag{23}$$

$$A_2 = \pi\cosh^4(\pi\varepsilon)(1-\beta^2)\frac{E^*R}{\Delta\gamma}\frac{(a+b)}{R} + \frac{\pi^2}{4(1-\beta^2)}\left(\frac{E^*R}{\Delta\gamma}\right)^2\left(\frac{a+b}{R}\right)^2 \times\left\{\left\{\sin\theta\left[\frac{(1+4\varepsilon^2)}{8}\frac{(a+b)}{R} - \frac{a+b}{2R}\frac{1}{1+\lambda}\right] - \frac{a+b}{R}\frac{\varepsilon\cos\theta}{1+\lambda}\right\}^2 - \left[\frac{(1+4\varepsilon^2)}{8}\frac{(a+b)}{R} - \frac{a+b}{2R}\frac{1}{1+\lambda}\right]^2 - \left(\frac{a+b}{R}\frac{\varepsilon}{1+\lambda}\right)^2\right\}, \tag{24}$$

and $a/b = \lambda$.

Actually, we should have the relation of $F^{\mathrm{R}} = F^{\mathrm{L}} = F$.

4 Analysis and discussion

According to the governing Eqs. (21) and (22), the pulling force F^{R} (or F^{L}) is a function of the contact width $a+b$. For a set of determined parameters θ, $E^*R/\Delta\gamma$, λ and β, the relation between $F^{\mathrm{R}}/\Delta\gamma$ (or $F^{\mathrm{L}}/\Delta\gamma$) and $(a+b)/R$ can be obtained numerically. The solution to $F^{\mathrm{R}} = F^{\mathrm{L}} = F$ at equilibrium corresponds to the intersection point of the two curves. This procedure can be repeated by choosing different values of λ (each value of λ results in a set of $F/\Delta\gamma$ and $(a+b)/R$ at equilibrium) until we get enough data points to plot the relation of $F/\Delta\gamma$ and $(a+b)/R$.

Figure 2 is a snapshot of intersection points for a given λ. One can see that the intersection points consist of stable and unstable solutions. Unstable solution corresponds to a negative derivative of the energy release rate G at contact edges, namely,

$$\frac{\partial G}{\partial(a+b)_{|F,\lambda}} < 0. \tag{25}$$

Figure 3 shows the normalized pulling force $F/\Delta\gamma$ as a function of normalized contact width $(a+b)/R$ for different pulling angle θ at equilibrium, in which the black dots denote the unstable solutions. The pull-off force and critical contact width at pull-off in the cases with different pulling angles can be found from the relation curves of $F/\Delta\gamma$ and $(a+b)/R$.

Figure 4 shows the relation of λ and θ at the moment of pull-off, from which one can see that λ asymptotically tends to 1 as the pulling angle θ increasing from 0 to $\pi/2$. Specially, λ becomes unity when $\theta = \pi/2$.

Deviations of the pull-off force and the critical contact width at pull-off in symmetric and asymmetric models are plotted in Figs. 5 and 6 for a set of given parameters,

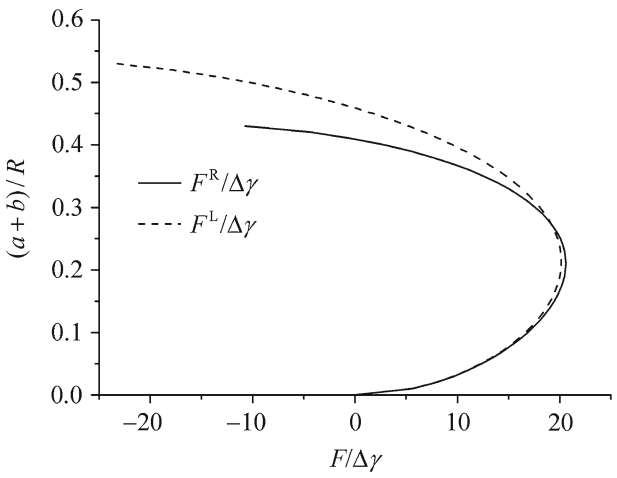

Fig. 2 Snapshot of intersection point for $\lambda = 1.09$ with $E^*R/\Delta\gamma = 1,000$, $\beta = 0.1$ and $\theta = \pi/6$. The intersection point denotes $F^{\mathrm{R}} = F^{\mathrm{L}} = F$

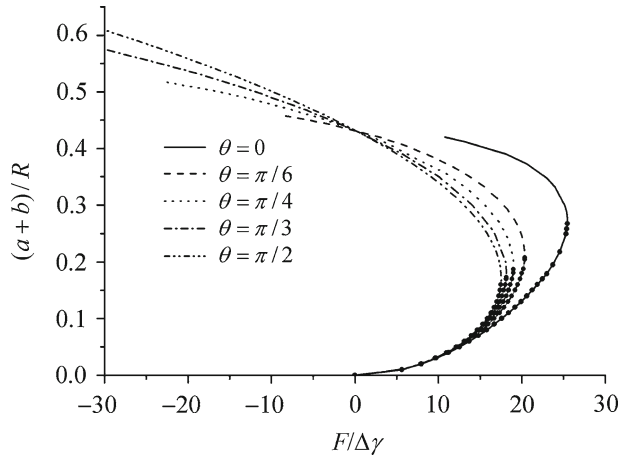

Fig. 3 Plots of relation of $F/\Delta\gamma$ as a function of $(a+b)/R$ for a set of parameters $E^*R/\Delta\gamma = 1{,}000$, $\beta = 0.1$ and different pulling angles $\theta = 0, \pi/6, \pi/4, \pi/3$ and $\pi/2$

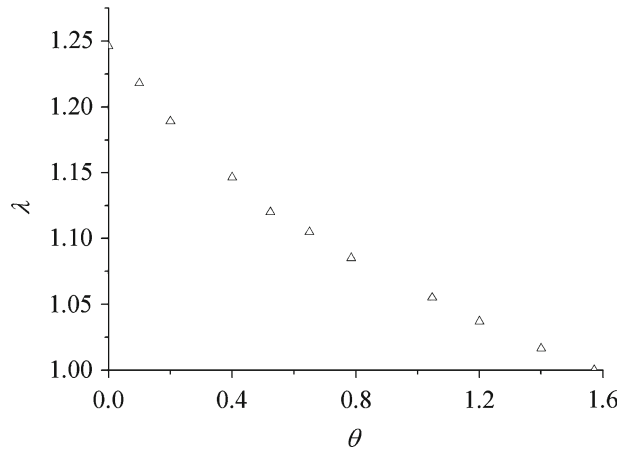

Fig. 4 The relation between λ and θ at the moment of pull-off for a set of parameters $E^*R/\Delta\gamma = 1{,}000$, $\beta = 0.1$

respectively. One can see that the deviation would be much smaller when θ changes from 0 to $\pi/2$.

In the same way, given a set of parameters $E^*R/\Delta\gamma$ and θ, we plot the normalized pulling force $F/\Delta\gamma$ as a function of the normalized contact width $(a+b)/R$ for different β in Fig. 7 and the corresponding relation between λ and β at the moment of pull-off in Fig. 8. From Fig. 8, one can see that the smaller of the absolute value of β, the closer the two contact lengths will be. The pull-off forces and the critical contact widths at pull-off in the symmetric and asymmetric models for different β are compared in Figs. 9 and 10, from which one can see that the smaller the absolute value of β is, the closer the results in the two models will be.

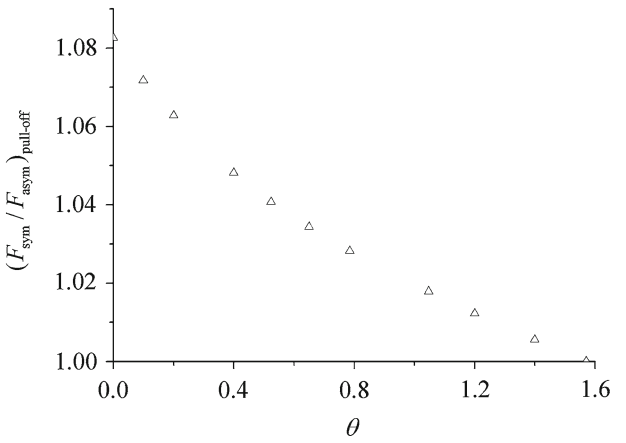

Fig. 5 Comparisons of the pull-off force F in the symmetric model to that in the asymmetric one with a set of given parameters $E^*R/\Delta\gamma = 1{,}000$, $\beta = 0.1$ and different pulling angles θ

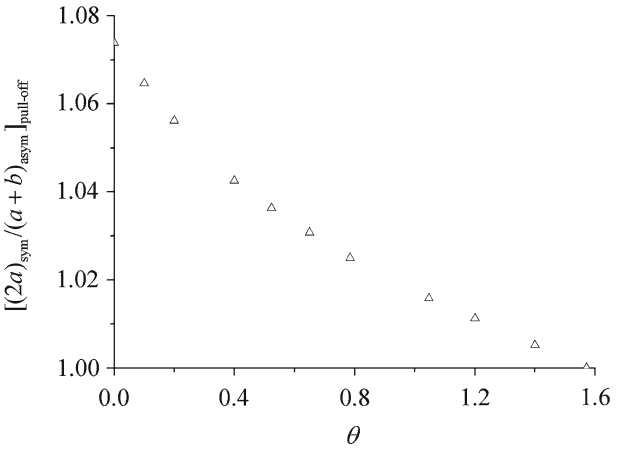

Fig. 6 Comparisons of the pull-off contact width $2a$ in the symmetric model to the one $a+b$ in the asymmetric model with a set of given parameters $E^*R/\Delta\gamma = 1{,}000$, $\beta = 0.1$ and different pulling angles θ

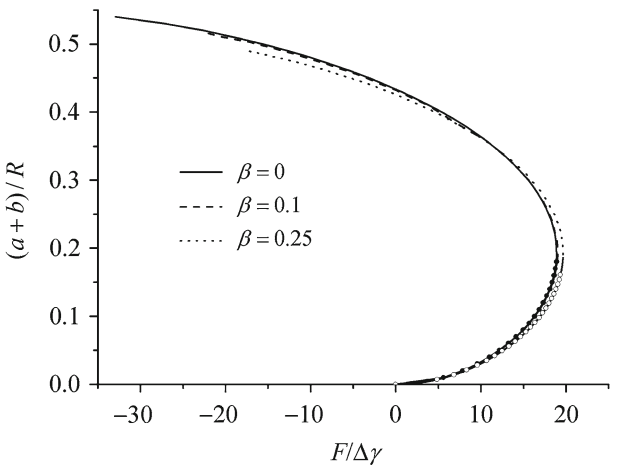

Fig. 7 Plots of the normalized pulling force $F/\Delta\gamma$ via the normalized contact width $(a+b)/R$ for $E^*R/\Delta\gamma = 1{,}000$, $\theta = \pi/4$ and different values of β

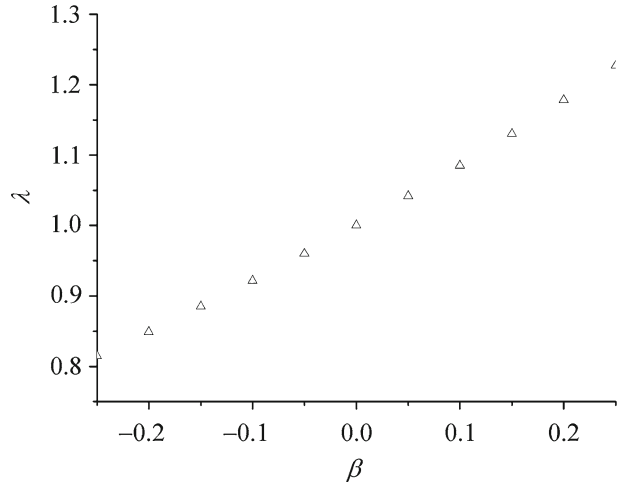

Fig. 8 The relation between λ and β at the moment of pull-off for a set of parameters $E^*R/\Delta\gamma = 1{,}000$, $\theta = \pi/4$

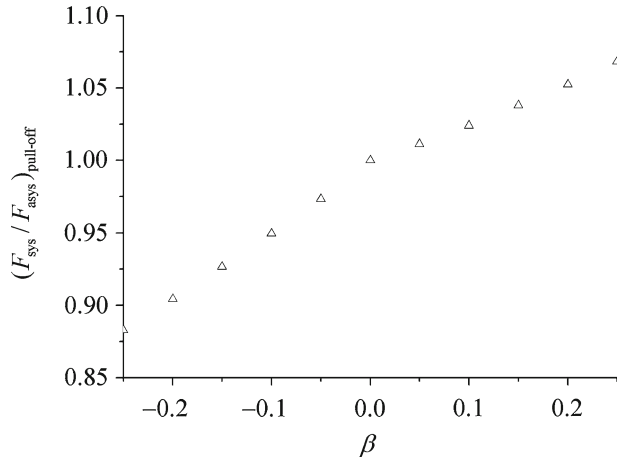

Fig. 9 Comparisons of the pull-off force F in the symmetric model to that in the asymmetric one with $E^*R/\Delta\gamma = 1{,}000$, $\theta = \pi/4$ and different values of β

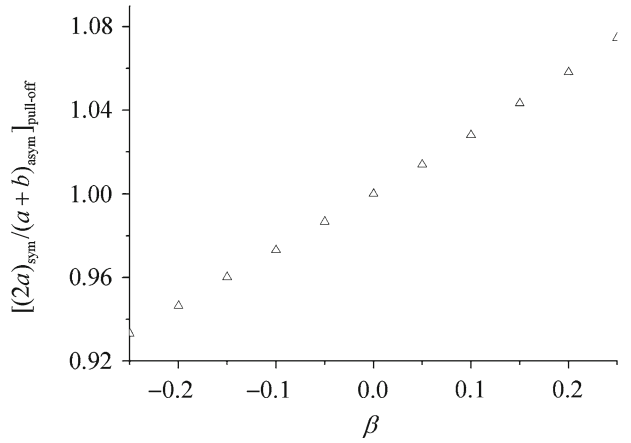

Fig. 10 Comparisons of the pull-off contact width $2a$ in the symmetric model to that in the asymmetric one with $E^*R/\Delta\gamma = 1{,}000$, $\theta = \pi/4$ and different values of β

5 Non-oscillatory solution

The above numerical analysis shows that the contact lengths a and b are equal when $\beta = 0$. In this section, analytical solution will be found for this case, i.e, $\beta = 0$, from which we have

$$r = \frac{1}{2}, \quad \varepsilon = 0. \tag{26}$$

Then the normal and tangential tractions on the contact interface can be written as

$$P(x) = -\frac{E^*\left[x^2 - \left(\frac{a-b}{2}\right)x - \frac{(a+b)^2}{8}\right]}{2R\sqrt{(b+x)(a-x)}} - \frac{F\sin\theta}{\pi\sqrt{(b+x)(a-x)}}, \tag{27}$$

$$Q(x) = -\frac{F\cos\theta}{\pi\sqrt{(b+x)(a-x)}}. \tag{28}$$

Then, the complex stress intensity factor can be de-coupled into two parts, i.e., purely mode I and mode II results.

$$K_{\mathrm{I}}^{\mathrm{R}} = -\sqrt{2\pi}\lim_{x\to a}(a-x)^{1/2}P(x) = \frac{\sqrt{\pi}E^*\left[a^2 - \left(\frac{a-b}{2}\right)a - \frac{(a+b)^2}{8}\right]}{\sqrt{2}R\sqrt{a+b}} + \frac{\sqrt{2}F\sin\theta}{\sqrt{\pi(a+b)}}, \tag{29}$$

$$K_{\mathrm{II}}^{\mathrm{R}} = -\sqrt{2\pi}\lim_{x\to a}(a-x)^{1/2}Q(x) = \frac{\sqrt{2}F\cos\theta}{\sqrt{\pi(a+b)}} \tag{30}$$

are the stress intensity factors for the right contact edge, i.e., at $x = a$.

$$K_{\mathrm{I}}^{\mathrm{L}} = -\sqrt{2\pi}\lim_{x\to -b}(b+x)^{1/2}P(x) = \frac{\sqrt{\pi}E^*\left[b^2 + \left(\frac{a-b}{2}\right)b - \frac{(a+b)^2}{8}\right]}{\sqrt{2}R\sqrt{a+b}} + \frac{\sqrt{2}F\sin\theta}{\sqrt{\pi(a+b)}}, \tag{31}$$

$$K_{\mathrm{II}}^{\mathrm{L}} = -\sqrt{2\pi}\lim_{x\to -b}(b+x)^{1/2}Q(x) = \frac{\sqrt{2}F\cos\theta}{\sqrt{\pi(a+b)}} \tag{32}$$

are the counterparts at $x = -b$.

Substituting Eqs. (29)–(32) into the following Griffith energy balance criterion

$$\frac{(K_{\mathrm{I}}^{\mathrm{R}})^2 + (K_{\mathrm{II}}^{\mathrm{R}})^2}{2E^*} = \Delta\gamma, \tag{33}$$

$$\frac{(K_{\mathrm{I}}^{\mathrm{L}})^2 + (K_{\mathrm{II}}^{\mathrm{L}})^2}{2E^*} = \Delta\gamma \tag{34}$$

yields

$$F^{\mathrm{R}} = -\frac{\pi E^* \sin\theta(3a-b)(a+b)}{16R} + \sqrt{\pi E^* \Delta\gamma (a+b) - \frac{\pi^2 E^{*2} \cos^2\theta (3a-b)^2 (a+b)^2}{256R^2}}, \tag{35}$$

$$F^{\mathrm{L}} = -\frac{\pi E^* \sin\theta(3b-a)(a+b)}{16R} + \sqrt{\pi E^* \Delta\gamma (a+b) - \frac{\pi^2 E^{*2} \cos^2\theta (3b-a)^2 (a+b)^2}{256R^2}}. \tag{36}$$

Using the relation $F^{\mathrm{R}} = F^{\mathrm{L}} = F$ yields an explicit solution as

$$a = b, \tag{37}$$

which is consistent with that in the numerical calculations.

Substituting the result in Eq. (37) into Eqs. (27) and (28) leads to the same results as those in the symmetric contact model [17]. The analytical solutions provided for the contact zone are obviously compatible with the equilibrium conditions in Eqs. (9).

6 Conclusions

A plain strain generalized JKR model of an elastic cylinder in adhesive contact with a half space is analyzed in the present paper. In the model, the external pulling force is acted on the elastic cylinder in an arbitrary direction, which results in an asymmetric contact width with respect to the axis of the structure. The results show that the smaller the absolute value of β or the larger the pulling angle θ, the more reasonable the symmetric model [17] would be to approximate the asymmetric one. When the pulling angle θ takes the value of $\pi/2$ or β equals zero, the symmetric model [17] is analytically proved to represent totally the asymmetric one.

References

1. Hertz, H.: On the contact of elastic solids. J. Reine Angewandte Math. **92**, 156–171 (1882)
2. Johnson, K.L., Kendall, K., Roberts, A.D.: Surface energy and the contact of elastic solids. Proc. R. Soc. Lond. A **324**, 301–313 (1971)
3. Kendall, K.: The adhesion and surface energy of elastic solids. J. Phys. D Appl. Phys. **4**, 1186–1195 (1971)
4. Derjaguin, B.V, Muller, V.M., Toporov, Y.P.: Effect of contact deformations on the adhesion of particles. J. Colloid Interface Sci. **53**, 314–326 (1975)
5. Maugis, D.: Adhesion of spheres: The JKR–DMT transition using a Dugdale model. J. Colloid Interface Sci. **150**, 243–269 (1992)
6. Chu, Y.S., Dufour, S., Thiery, J.P., Perez, E., Pincet, F.: Johnson-Kendall-Roberts theory applied to living cells. Phys. Rev. Lett. **94**, 028102 (2005)
7. Chen, S., Gao, H.: Non-slipping adhesive contact between mismatched elastic spheres: A model of adhesion mediated deformation sensor. J. Mech. Phys. Solids **54**, 1548–1567 (2006)
8. Chen, S., Gao, H.: Non-slipping adhesive contact of an elastic cylinder on stretched substrates. Proc. R. Soc. Lond. A **462**, 211–228 (2006)
9. Arzt, E., Gorb, S., Spolenak, R.: Form micro to nano contacts in biological attachment devices. Proc. Natl. Acad. Sci. USA **100**, 10603–10606 (2003)
10. Glassmaker, N.J., Jagota, A., Hui, C.Y., Kim, J.: Design of biomimetic fibrillar interface: 1. Making contact. J. R. Soc. Interface **1**, 23–33 (2004)
11. Hui, C.Y., Glassmaker, N.J., Tang, T., Jagota, A.: Design of biomimetic fibrillar interface: 2. mechanics of enhanced adhesion. J. R. Soc. Interface **1**, 35–48 (2004)
12. Gao, H., Wang, X., Yao, H., Gorb, S., Arzt, E.: Mechanics of hierarchical adhesion structures of gecko. Mech. Mater. **37**, 275–285 (2005)
13. Spolenak, R., Gorb, S., Gao, H., Artz, E.: Effects of contact shape on the scaling of biological attachments. Proc. R. Soc. A. **46**, 305–319 (2005)
14. Chen, S., Gao, H.: Non-slipping adhesive contact between mismatched elastic cylinders. Int. J. Solids Struct. **44**, 1939–1948 (2007)
15. Chen, S., Gao, H.: Bio-inspired mechanics of reversible adhesion: Orientation-dependent adhesion strength for non-slipping adhesive contact with transversely isotropic elastic materials. J. Mech. Phys. Solids **55**, 1001–1015 (2007)
16. Chen, S., Soh, A.: Tuning the geometrical parameters of biomimetic fibrillar structures to enhance adhesion. J. R. Soc. Interface **5**, 373–382 (2008)
17. Chen, S., Wang, T.: General solution to two-dimensional non-slipping JKR model with a pulling force in an arbitrary direction. J. Colloid Interface Sci. **302**, 363–369 (2006)
18. Johnson, K.L.: Contact Mechanics. Cambridge University Press, New York (1985)
19. Yao, H., Della Rocca, R., Guduru, P.R., Gao, H.: Adhesion and sliding response of a biologically inspired fibrillar surface: Experimental observations. J. R. Soc. Interface **5**, 723–733 (2008)
20. Dundurs, J.: Edge-bonded dissimilar orthogonal elastic wedges. Appl. J. Mech. **36**, 650–652 (1969)